Analysis of γ'/γ Equilibrium in Ni-Al-X Alloys by the Cluster Variation Method with the Lennard-Jones Potential

MASATO ENOMOTO and HIROSHI HARADA

Various characteristics of γ'/γ phase equilibrium in ternary Ni-Al-X alloys are analyzed by the cluster variation method (CVM) with the phenomenological Lennard-Jones pair potential. Among the eleven alloy elements studied, three types of substitution behavior in γ', *i.e.*, the preferential substitution for Ni sites (Co and Cu), the almost entire substitution for Al sites (Ti, Nb, Mo, Hf, Ta, and W), and the substitution for both (Cr, Mn, and Fe), are recognized depending upon the relative magnitude of the Ni-X and Al-X interactions. In the last type, the substitution site appears to depend remarkably upon the Al and/or X concentrations in γ': while X atoms enter preferentially, the Al sublattice in the case that the sum of the two concentrations is less than the stoichiometry composition (0.25), they begin to enter the Ni sublattice as the sum exceeds it. The predicted substitution behavior is in good agreement with direct and indirect experimental evidences thus far reported. The direction of γ'/γ equilibrium phase boundaries, the equilibrium partition coefficient of X, and the effects of alloying upon the order-disorder transformation temperature from metastable γ' to γ all appear to be closely related to substitution behavior. Also, the variation of lattice constants of γ' and γ with the alloy element concentration may be better understood by collation with the substitution sites or the short range order in each phase.

I. INTRODUCTION

UNDERSTANDING the alloying effects upon the characteristics of γ'/γ phase equilibrium is of vital importance for the development of Ni base superalloys of superior high temperature performance. Hence, numerous constitutional data, such as phase equilibrium compositions, partition coefficients, and lattice parameters and so forth, have been hitherto accumulated in many ternary Ni-Al-X and higher order systems. Recently more attention has been drawn to refractory elements to seek further improvement of the resistance to creep rupture at high temperatures.

Compared to experiment, much less theoretical efforts appear to have been made to investigate the characteristics of phase equilibrium in Ni base superalloys. In the regular solution model developed by Kaufman *et al.*,[1–4] intermetallic compounds are treated either as a line compound or in the same manner as the solid solution in the case that they have a finite stability composition range. In the latter treatment the two sublattices forming γ' are not distinguished. In contrast, it has been demonstrated by Sanchez *et al.*[5] that the cluster variation method with the Lennard-Jones pair potential is capable with sufficient accuracy of describing the γ'/γ phase equilibrium in the binary Ni-Al system, given data on the cohesive energy of component species and the lattice parameter at some compositions in the relevant phases of binary systems.

This method assumes in effect that the lattice strains which are introduced upon alloying are uniform, though they in fact may be localized around the solute atoms. As a result, a significant amount of error may be involved in the evaluation of internal energies and so forth.[6]* Also, the coherency strains in the vicinity of γ'/γ interfaces, which are likely to affect significantly the characteristics of phase equilibrium, are not taken into account. However, because the lattice constant, an important parameter which governs the creep resistance of superalloys, is explicitly included, the effect of alloying upon lattice constants can be analyzed simultaneously with other characteristics of phase equilibrium. Thus, this method seems to be most appropriate at this time for promoting our understanding the effects of alloying element upon the γ'/γ equilibrium and its modeling in higher order systems to achieve more accurate and complete predictions of microstructures and mechanical properties of Ni base superalloys than the hitherto available one, for example, the method based upon the multiple linear regression analyses.[9,10] In fact, an attempt to extend this analysis to a few ternary or even higher order systems has already been reported.[11]

Guard and Westbrook[12] were the first authors to deduce the substitution site of various alloy elements in γ' from the appearance of the γ' phase field in the isothermal section of ternary phase diagram. The proposed correlation of the substitution site with the appearance of the γ' phase field may indicate that the substitution behavior not only affects the mechanical properties of γ' itself, but also has an important influence upon the characteristics of γ'/γ ternary phase equilibrium. Hence, in this report a considerable emphasis is placed upon the analysis of the substitution site of alloy element in γ' and its comparison with the experimental results as well, *e.g.*, Mössbauer spectroscopy[13,14] and ALCHEMI (Atom Location by Channeling Enhanced Microanalysis),[15]

*A different approach based upon a polynomial expansion for the expression of energies has been used to extend the analysis to the entire composition in some binary systems.[7,8]

MASATO ENOMOTO and HIROSHI HARADA are Senior Researchers, Materials Physics Division and Materials Design Division, respectively, National Research Institute for Metals, 2-3-12, Nakameguro, Meguroko, Tokyo 153, Japan.

Manuscript submitted July 19, 1988.

which yield more direct results compared to the deductions from the appearance of the phase field.[12,16]

II. METHOD OF CALCULATIONS

A. *Free Energy of γ′ and γ Phases*

The procedures of calculation are exactly the same as those described previously.[5,17] Only the nearest neighbor pair interactions are assumed to have significant contributions to the energy of both $\gamma'(L1_2)$ and γ(fcc) phases. Under such an assumption, the tetrahedron approximation may be adequate for calculating the entropy of the system. The entropy per each lattice point is written as

$$S_{\gamma'} = -k\left(\sum_{ijkl} 2L(z_{ijkl}^{ABBB}) - 3\sum_{ij}\{L(y_{ij}^{AB}) + L(y_{ij}^{BB})\} + \frac{5}{4}\sum_{i}\{L(x_i^A) + 3L(x_i^B)\}\right) \quad [1a]$$

and

$$S_{\gamma} = -k\left(\sum_{ijkl} 2L(z_{ijkl}) - 6\sum_{ij} L(y_{ij}) + 5\sum_{i} L(x_i)\right) \quad [1b]$$

for γ' and γ phases, respectively. Here, the superscripts A and B denote the Al and Ni sublattices, respectively. Then, z_{ijkl}^{ABBB} (or z_{ijkl}) is the probability of finding atoms i, j, k, and l in a tetrahedron nearest neighbor atom cluster in γ' (or γ) as shown in Figure 1; y_{ij}^{AB} (or y_{ij}), the probability of finding the i and j atoms in a nearest neighbor atom pair; x_i^A (or x_i), the probability of finding the i atom at one lattice point; k the Boltzmann constant, and $L(\zeta) = \zeta \ln \zeta - \zeta$. The summation extends from 1 to 3 (1, 2, and 3 for Ni, Al, and X, respectively). It is also assumed that the energy is expressed by the sum of the nearest neighbor pair interactions, namely,

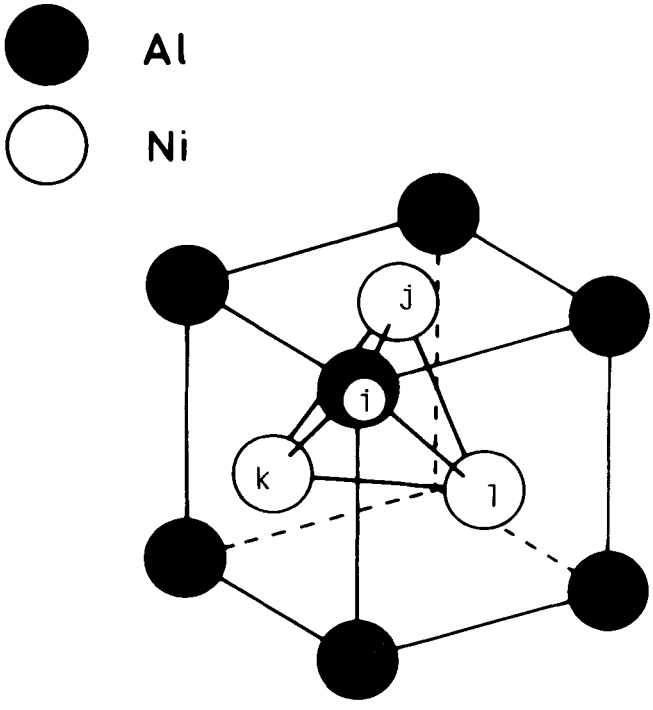

Fig. 1—Tetrahedron cluster for fcc structure used in the calculation.

$$H_{\gamma'} = \frac{w_1}{4}\sum_{ij} e_{ij}(r)(y_{ij}^{AB} + y_{ij}^{BB}) \quad [2a]$$

and

$$H_{\gamma} = \frac{w_1}{2}\sum_{ij} e_{ij}(r) y_{ij} \quad [2b]$$

where w_1 is the nearest neighbor coordination number in the fcc lattice. The pair energy $e_{ij}(r)$ is dependent upon the interatomic distance, r, and thereby, the concentration dependence of atom interaction is incorporated.

In order to obtain the most probable atom configuration at equilibrium, the grand potential of the system defined as

$$\Omega = H - TS + PV + \sum_i \mu_i x_i \quad [3]$$

is minimized with respect to both z_{ijkl}^{ABBB} (or z_{ijkl}) and the atomic volume, V, namely, the atom distance, at constant temperature, T, pressure, P, and the chemical potential of the i atom, μ_i, under the normalization condition, *i.e.*, $\Sigma_{ijkl} z_{ijkl}^{ABBB} = 1$. As a result, the most probable atom configuration in the tetrahedron cluster for γ' is expressed as

$$z_{ijkl}^{ABBB} = \exp\left(\frac{\beta\lambda}{2}\right) \exp\left[-\frac{\beta}{2}\left(u_{ijkl} - \frac{\mu_i + \mu_j + \mu_k + \mu_l}{4}\right)\right] \times (y_{ij}^{AB} y_{ik}^{AB} y_{il}^{AB} y_{jk}^{BB} y_{jl}^{BB} y_{kl}^{BB})^{1/2} \times (x_i^A x_j^B x_k^B x_l^B)^{-5/8} \quad [4a]$$

$$u_{ijkl} = e_{ij}(r) + e_{ik}(r) + e_{il}(r) + e_{jk}(r) + e_{jl}(r) + e_{kl}(r) \quad [5]$$

where λ is the Lagrange multiplier introduced to take into account the normalization condition, and $\beta = 1/kT$. Also, the equilibrium nearest neighbor atom distance is calculated from the equation,

$$\frac{w_1}{4}\sum_{ij}\frac{de_{ij}}{dV}(y_{ij}^{AB} + y_{ij}^{BB}) = -P \quad [6a]$$

The corresponding equations for γ are, respectively,

$$z_{ijkl} = \exp\left(\frac{\beta\lambda}{2}\right) \exp\left[-\frac{\beta}{2}\left(u_{ijkl} - \frac{\mu_i + \mu_j + \mu_k + \mu_l}{4}\right)\right] \times (y_{ij} y_{ik} y_{il} y_{jk} y_{jl} y_{kl})^{1/2} \times (x_i x_j x_k x_l)^{-5/8} \quad [4b]$$

$$\frac{w_1}{2}\sum_{ij}\frac{de_{ij}}{dV} y_{ij} = -P \quad [6b]$$

The pair interactions are expressed by the Lennard-Jones potential of the form,[18]

$$e_{ij}(r) = e_{ij}^0 \left[\left(\frac{r_{ij}}{r} \right)^{m_{ij}} - \left(\frac{m_{ij}}{n_{ij}} \right) \left(\frac{r_{ij}}{r} \right)^{n_{ij}} \right] \quad [7]$$

Following Sanchez *et al.*,[5] m_{ij} and n_{ij} are put equal to 8 and 4 which are close to the average value of the exponent of pure metals. The potential parameters r_{ij} corresponds to the interatomic distance at which $e_{ij}(r)$ reaches its minimum, *i.e.*, the most negative value, $-e_{ij}^0$. The most probable configuration and the equilibrium atom distance in each phase are calculated by incorporating Eqs. [6] into the successive iteration scheme called the Natural Iteration technique.[19] The substitution site of X in γ' can be known from x_3^A (or x_3^B) for given P, T, and μ_i values. The characteristics of γ'/γ phase equilibrium are calculated from most probable atom configurations of each phase which yield the same value of Ω under the same values of P, T, μ_i in the two phases. The transformation temperature from metastable γ' to γ is determined as the minimum temperature at which the atom configuration becomes the same in the two sublattices of γ'.

B. *Determination of Parameter Values*

The values of the L-J potential parameters are evaluated in principle in the same manner as used in the analysis of the binary system. For fcc metals,

$$e_{ii}^0 = -\frac{2}{w_1} H_i \quad [8]$$

$$r_{ii} = \frac{a_i}{\sqrt{2}} \quad [9]$$

where H_i and a_i are the enthalpy and the lattice parameter of pure i metal, respectively. The data on H_i of metals, alloys, and compounds are available in the compilation by Hultgren *et al.*[20,21] and those on a_i, in Pearson[22] and its recent much enlarged edition.[23] For elements which do not form the fcc lattice at relevant temperatures, H_i for metastable fcc phase was estimated from the latent heat of allotropic transformation[20] or the lattice stability parameter compiled by Kaufman[24] and Kaufman and Nesor.[25] Because the change in the specific volume associated with the allotropic transformation is usually not very significant,[26] r_i of such elements was calculated assuming that the specific volume is not changed upon transformation. The values for pure metals thus determined are shown in Tables I(a) and (b). In Table I(b) the superscripts h, b, and cb indicate that the element takes hcp, bcc, and complex bcc structures at room temperature, respectively.

In the system in which an $L1_2$ type compound (isomorphous to γ') is reported to exist, the Ni-X interaction parameters can be calculated from equations,

$$r_{ij} = \frac{a_{Ni}}{\sqrt{2}} \left(\frac{H_i - 2\alpha^8 H_{ij}^c}{H_i - 2\alpha^4 H_{ij}^c} \right)^{1/4} \quad [10]$$

$$e_{ij}^0 = \frac{2}{w_1} \frac{(H_i - 2\alpha^4 H_{ij}^c)^2}{H_i - 2\alpha^8 H_{ij}^c} \quad [11]$$

where H_{ij}^c and a_{ij}^c are, respectively, the heat of formation

Table I. Lennard-Jones Potential Parameters for (*a*) Binary and (*b*) Ternary Ni-Al-X Systems

	i-j	e_{ij}^0/e_{11}^0	r_{ij}/r_{11}
(a)			
	Ni-Al		
	γ'-Ni_3Al	1.047	1.023
	γ-Ni	1.058	1.019
	"BF"	1.000	1.053
	Al-Al	0.766	1.149

Ne_{11}^0 = 17.13 kcal/mole, r_{11} = 2.491 Å

	Alloying Element	e_{ij}^0/e_{11}^0 Ni-X	e_{ij}^0/e_{11}^0 Al-X	e_{ij}^0/e_{11}^0 X-X	r_{ij}/r_{11} Ni-X	r_{ij}/r_{11} Al-X	r_{ij}/r_{11} X-X
(b)							
	Ti	1.184	1.109	1.095^h	1.035	1.122	1.174
	Cr	0.982	0.790	0.902^b	1.018	1.073	1.032
			(0.760)*	(0.780)			
	Mn	0.908^c	0.839	0.659^{cb}	1.036^c	1.066	1.096
	Fe	1.057^c	0.931	0.964	1.017^c	1.031	1.014
			(0.790)	(0.924)			
	Co	1.002	0.910	0.998	1.007	1.009	1.006
	Cu	0.886	0.858	0.785	1.015	1.049	1.026
	Nb	1.488	1.298	1.656^b	1.038	1.171^v	1.181
	Mo	1.285	1.035	1.506^b	1.028	1.147^v	1.115
				(1.700)			
	Hf	1.450^m	1.129^m	1.450^h	1.058^v	1.236^v	1.293
	Ta	1.543^m	1.262^m	1.797^b	1.049^v	1.165^v	1.180
	W	1.460	1.238	1.960^b	1.029	1.150^v	1.132

*The values in the parentheses are the ones which bring calculated and measured phase boundaries into close agreement. They are designated as the "BF" values in the text.

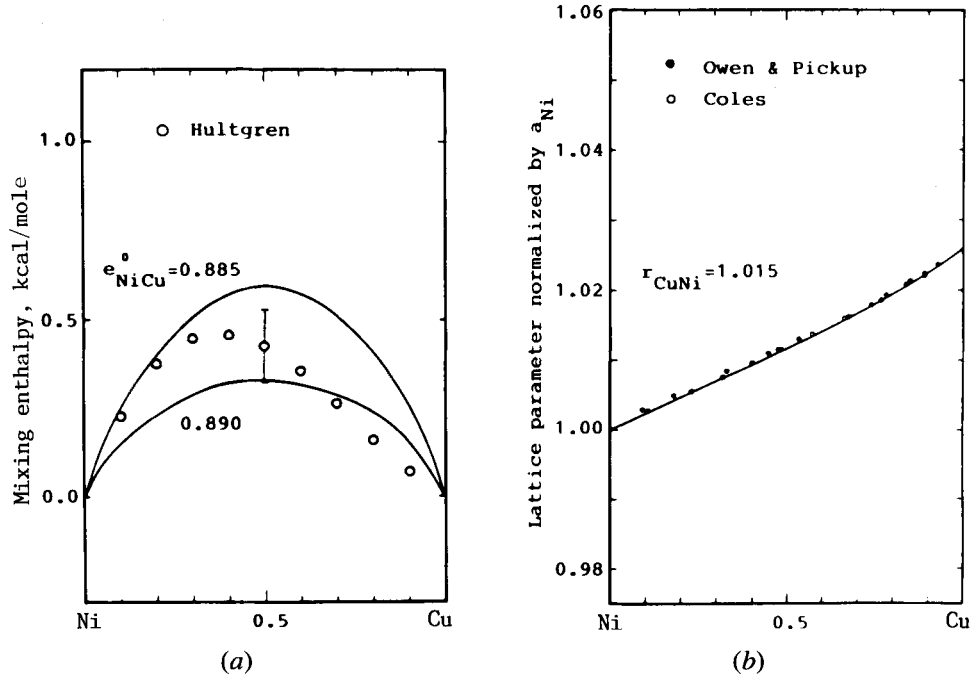

Fig. 2—Determination of Lennard-Jones potential parameters of Ni-Cu interaction: (*a*) e^0_{NiCu}; (*b*) r_{NiCu}. Data were taken from Hultgren[21] and Pearson,[22] respectively.

and the lattice parameter of the compound, and $\alpha = a^c_{ij}/a_{Ni}$. The interaction parameters thus determined are denoted by the superscript *c* in Table I(b).

In the majority of the systems, no $L1_2$ compound has been reported to exist. In such systems the parameters are determined by best fitting the enthalpy and the lattice parameter of the fcc solid solution. The parameter values were initially guessed assuming binary regular solution behavior and then more precise values were determined performing calculations following the procedures described in Section II–A for binary systems. In Figures 2 and 3 are shown examples of determining the Ni-Cu

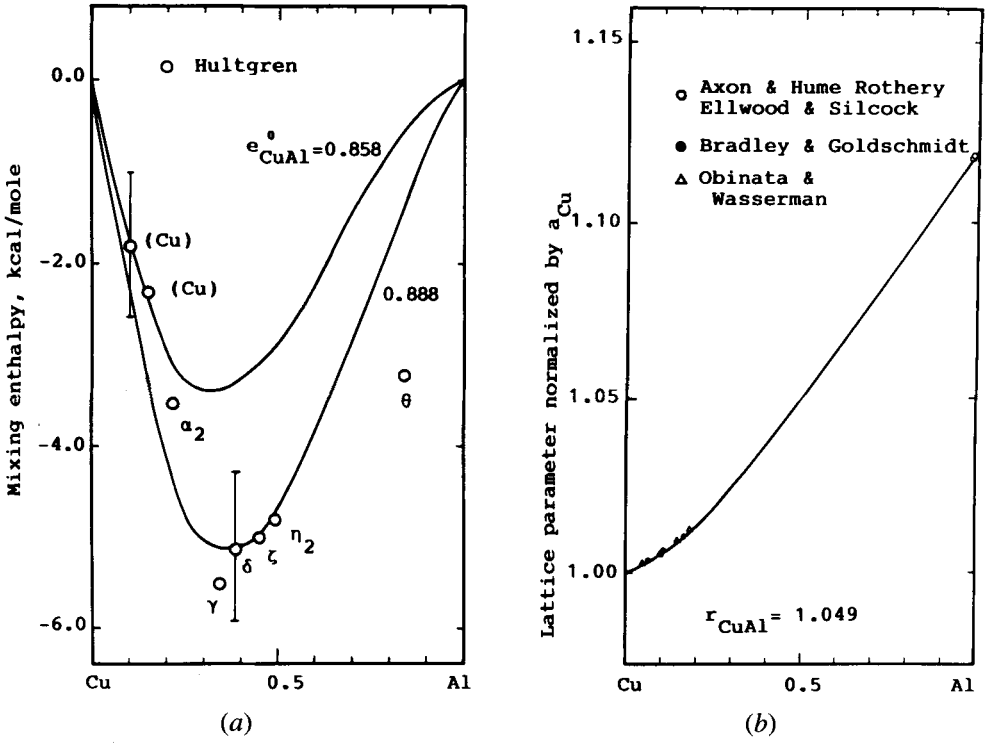

Fig. 3—Determination of Lennard-Jones potential parameters for Al-Cu interaction: (*a*) e^0_{AlCu}; (*b*) r_{AlCu}.

and Al-Cu interaction parameters. Because the influence of one parameter upon the other was usually insignificant (*i.e.*, the e_{ij}^0 value did not affect the r_{ij} value and *vice versa*), the value of each parameter can be readily obtained by this procedure. The thermochemical data are not available for Ta and Hf. Accordingly, the semiempirical method proposed by Miedema *et al.*[27,28] was used to evaluate the heat of mixing, H_{ij}, for these elements (superscript m in Table I(b)). Also, the Vegard's law was assumed to estimate the lattice parameter of the solid solution, a_{ij}, when no data appear to be available (superscript v).

The parameter values of Ni-Al interaction are shown in Table I(a). Those evaluated from the data of enthalpy) and lattice parameter of γ'-Ni_3Al and γ-Ni are reasonably close. The values designated as "BF" are the ones which yield best fit to the γ'/γ boundary compositions in the binary system, which are very similar to those previously reported.[5]

It is difficult to determine precisely the error limits of these parameter values. The errors in the original enthalpy and lattice parameter data may be inherited in them. For example, ±15 and ±2 pct errors in e_{ij}^0 and r_{ij} values, respectively, considerably alter the numerical results for some elements, particularly those designated as Type III elements (Section III–A). The differences resulted from the ranges of parameter values will be mentioned as much as possible when they are considered to be significant. In the calculations the interaction parameters normalized by e_{11}^0 and r_{11} are all assumed to be temperature independent, which implies that one assumes the same temperature dependence of the enthalpy and lattice parameter as that of pure Ni. The error involved in such a procedure is likely to be less than a few percent for both H_{ij} and a_{ij}.

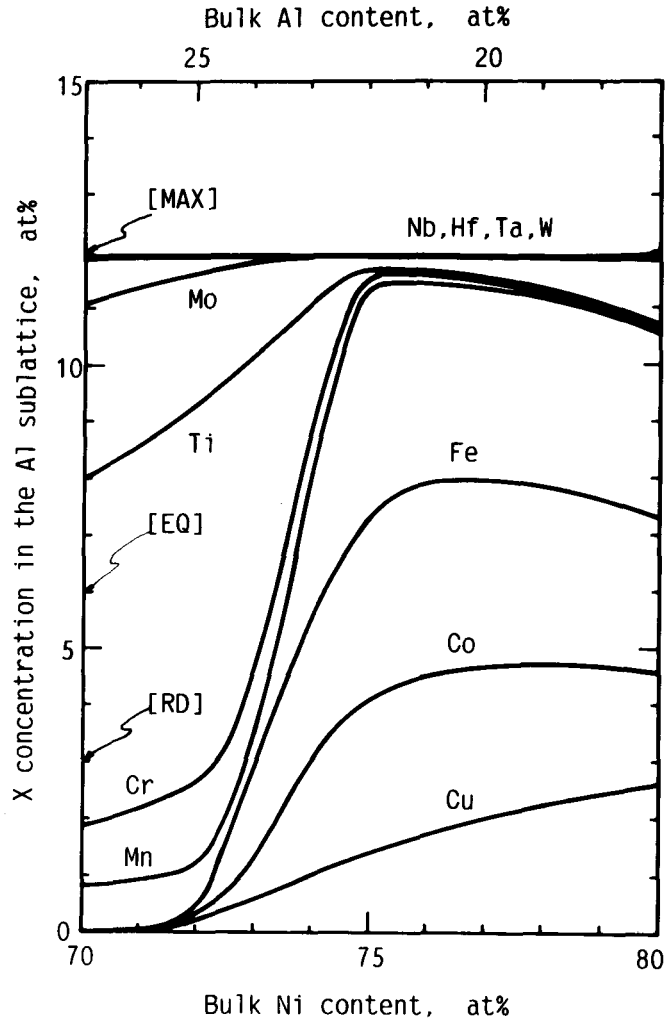

Fig. 4—Variation of alloy element concentration in the Al sublattice with Ni (or Al) concentration in γ'. The bulk alloy element concentration is 3 at. pct.

III. RESULTS AND DISCUSSION

A. *Preferential Substitution Lattice of X in γ'*

In Figure 4 is shown the calculated variation of the X concentration in the Al sublattice of γ', x_3^A, at 1000 °C. The bulk concentration of X is 3 at. pct. The fraction of occupancy of Al sites is seen to vary greatly from one alloy element to another. The symbols [MAX], [EQ], and [RD] denote the concentrations of X for the cases in which all atoms are substituted for Al, an equal number of atoms enter the two lattices, and atoms are randomly distributed in the two lattices, respectively. It is seen that Nb, Hf, Ta, and W are substituted almost entirely for Al. Titanium and Mo are mostly substituted for Al for Ni concentrations larger than the stoichiometry ($x_{Ni} > 0.75$). However, small amounts of these atoms begin to enter the Ni sublattice as the Ni concentration becomes less than the stoichiometry, *i.e.*, when the Al lattice is filled up with Al and/or these atoms.

The proportion of Cr, Mn, and Fe atoms entering the Ni sublattice is increased in this order in the Ni-lean side of stoichiometry. On the other hand, in the Ni-rich side, Cr and Mn atoms mostly enter the Al sublattice. A little more than half of Fe atoms are seen to enter the Al sublattice. In the same composition range, Co is substituted for Al with *larger* probability than random, but the number of Co atoms in the Al lattice is *less* than that in the Ni sublattice. Copper preferentially enters the Ni sublattice. Hereafter, substitution behavior is classified into three groups: Type I elements which are preferentially substituted for Ni (Co and Cu); Type II elements which are almost entirely substituted for Al (Ti, Nb, Mo, Hf, Ta, and W); and Type III elements of which the substitution site is remarkably changed on both sides of stoichiometry (Cr, Mn, and Fe).

The above classification seems to be in good agreement with the substitution sites of each element hitherto accepted, as summarized by some authors.[12,16,29] However, some discrepancies are observed: from the shape of the γ' phase field Mn was regarded as wholly substituted for Al;[12] the results from X-ray diffractometry *etc.* tend to favor the substitution of Mo and W for both Ni and Al sites.[30,31,32] In these comparisons the differences in bulk compositions of γ' were ignored. One of the greatest advantages of the present analysis may be that the concentration dependence of substitution behavior is readily analyzed.

The variations of calculated x_3^A of Fe, Cr, and Co with

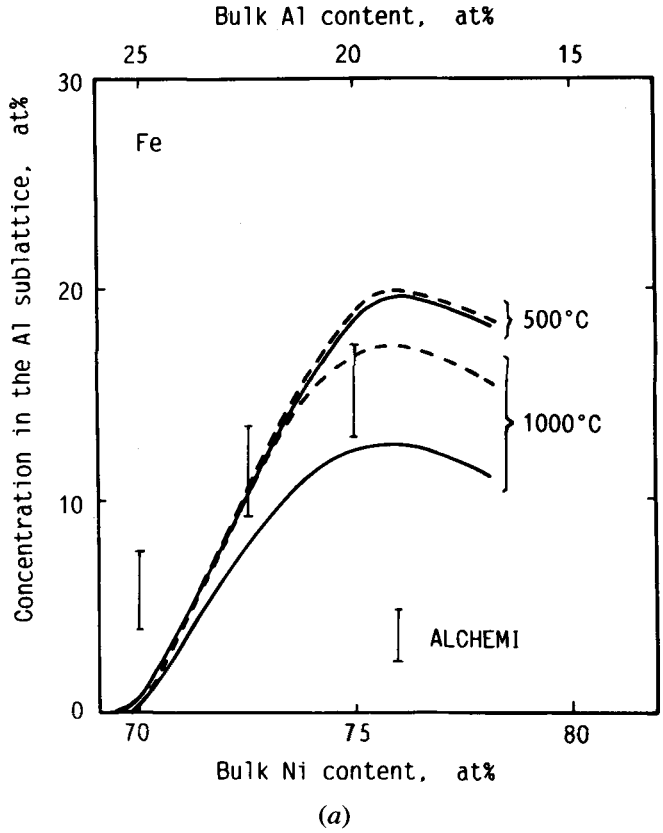

(*a*)

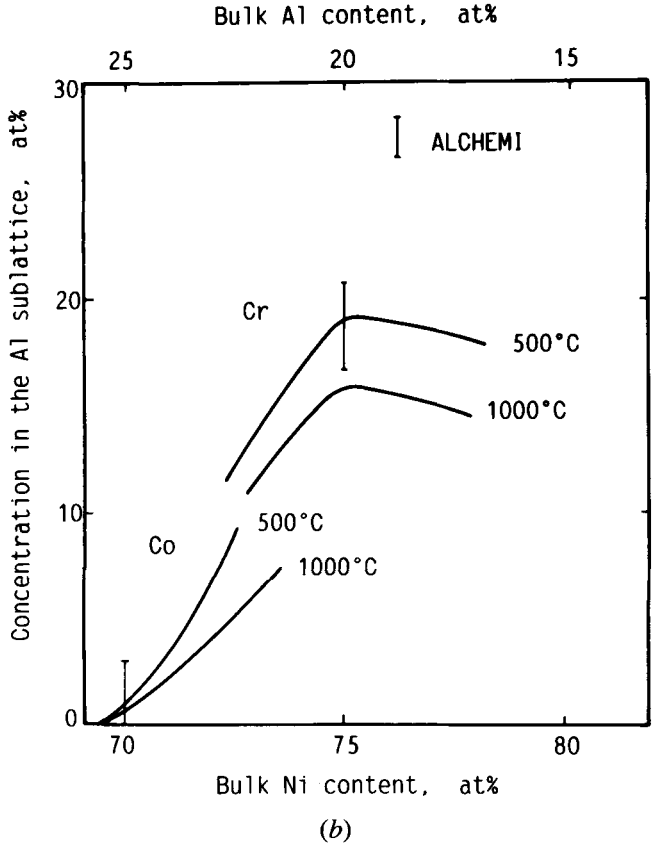

(*b*)

Fig. 5—Comparison of calculated (*a*) Fe and (*b*) Cr and Co concentrations in the Al sublattice with those measured by ALCHEMI.[15] Dashed curves are calculated with the use of the "BF" values in Table I(b).

the Ni (or Al) content are compared with those measured by means of electron channeling (ALCHEMI)[15] in Figures 5(a) and (b). The bulk concentrations of these elements in γ' are all approximately 5 at. pct. The temperature at which the atom distribution was actually quenched was not determined in this experiment. Accordingly, the calculations were performed at two temperatures, *i.e.*, 500 and 1000 °C. The solid and dashed curves are calculated, respectively, using the parameter values determined in Section II–B and the values which best fit the reported γ'/γ equilibrium phase boundaries (Section III–B; in Table I(b), they are shown in the parentheses and hereafter denoted "BF"). The difference in the two curves at 1000 °C is large. Though the measured x^A_{Fe} is considerably larger than the calculations at the lowest Ni content ($Ni_{70}Al_{25}Fe_5$), the observed variation of x^A_{Fe} with the bulk Ni concentration is exactly the one predicted from the calculation. As seen in Figure 5(b), the agreement between theory and experiment is very good also for Cr and Co. The two sets of parameter values yielded very similar results for Cr.

The occupancy fraction of Fe and Co in the Al sublattice was also measured by means of the Mössbauer spectroscopy.[13,14] As shown in Table II, whereas the x^A_{Fe} back-calculated from the measured occupancy fraction tends to be somewhat higher than the calculated ones, agreement is appreciably improved (the number in the parentheses) if one used the "BF" values in Table I(b). However, it is not clear whether structural vacancies are present at an off-stoichiometry composition of $L1_2$ ordered compounds, as reported for some B2 type compounds,[33] or, if they are, significantly affect substitution behavior of these elements.

The existence of various types of substitution behavior can be interpreted simply from the relative magnitude of the potential of each atom pair. In the following it is assumed that structural vacancies do not exist in γ'. Figure 6 shows the calculated $e_{13}(r)$ and $e_{23}(r)$ (both normalized by e^0_{11}) as a function of the bulk Ni content in γ' for Cu, Cr, and Nb, which represent each type of substitution behavior, respectively. For Nb, the Ni-Nb interaction (e_{13}) may be much more negative than the Al-Nb interaction (e_{23}). Hence, it is energetically much more favorable for this element to be substituted for Al and surrounded by twelve first neighbor Ni atoms. Thus, most Type II elements exhibit almost entire substitution for

Table II. Comparison of the Mössbauer Spectroscopy Data on the Site Occupancy of Fe Atoms in Ni_3Al with the CVM Calculation

	Fraction of Fe Atoms in the Al Sublattice*	x^A_{Fe} Back-Calculated from the Measured Occupancy Fraction	CVM Calculated x^A_{Fe} at 1000 °C
$Ni_{73.8}Al_{23.8}Fe_{2.5}$	0.78	0.08	0.041 (0.045)
$Ni_{70.3}Al_{20.4}Fe_{9.3}$	0.54	0.20	0.126 (0.185)

*The specimens were homogenized at 1000 °C for 24 h.[14]

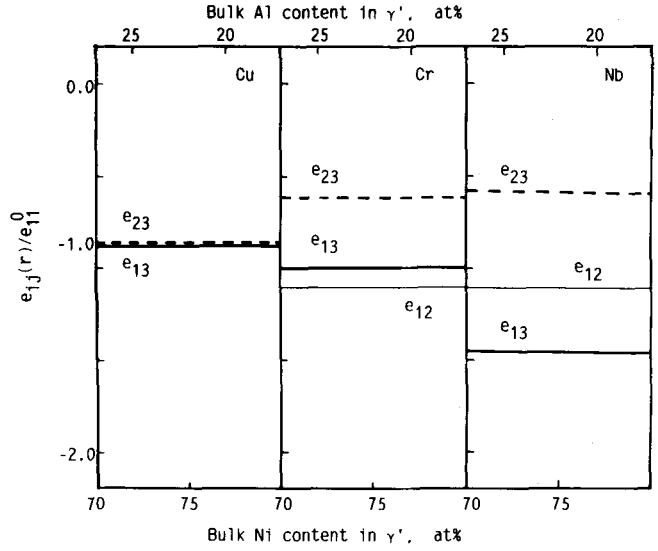

Fig. 6—Comparison of Ni-X(e_{13}), Al-X(e_{23}), and Ni-Al(e_{12}) pair potentials for three X representing each type of substitution behavior.

Al. For Cu e_{13} is only slightly more negative than e_{23}. This element may be substituted for Ni, because the Ni sublattice has three times more lattice points than the Al sublattice and, thereby, entering the Ni sublattice may be favored in terms of the configurational entropy. The tendency of Cu to occupy Ni sites is not so strong as

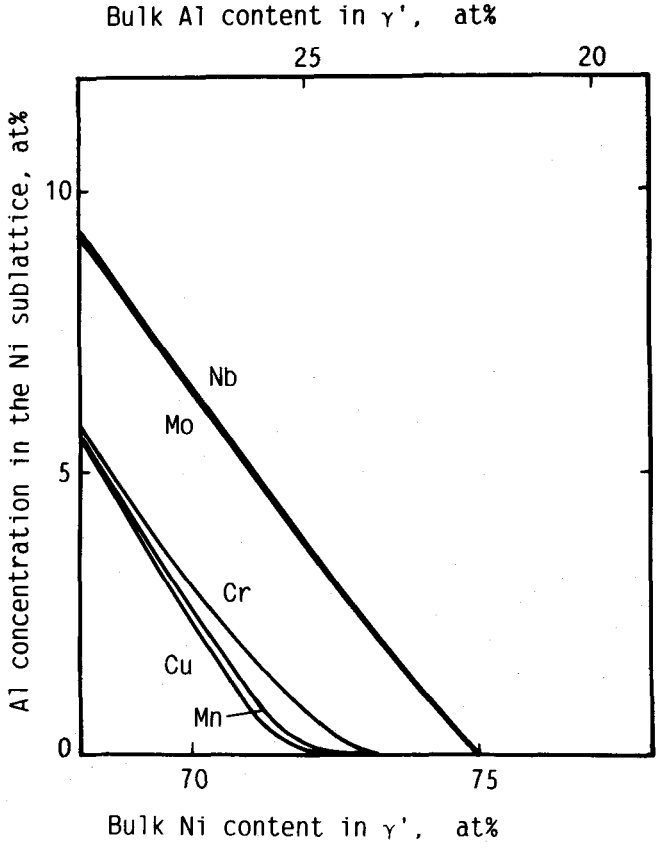

Fig. 7—Variation of Al concentration in the Ni sublattice with the Ni (or Al) concentration in γ'. The bulk alloy element concentration is 3 at. pct.

that of the Type II elements to occupy Al sites and, thus, the substantial fraction of the Type I elements may enter the Al sublattice (Figure 4).

The difference in the Ni-Cr and Al-Cr pair potentials is intermediate between those of Nb and Cu. As stated earlier, Cr atoms are preferentially substituted for Al when $x_{Al} + x_{Cr} < 0.25$. When the sum of the two concentrations exceeds 0.25, the question may arise as to which atoms are squeezed out of the Al sublattice. In Figure 7 the calculated Al concentration in the Ni sublattice, x^B_{Al}, is plotted over the composition range which encompasses the stoichiometry of several ternary γ'. In γ' containing Nb and Mo, Al begins to enter in the Ni sublattice as soon as x_{Ni} becomes less than 0.75. This is because squeezing out of Al into the Ni sublattice may be energetically more favorable on account of a more negative e_{13} value than e_{12} (Ni-Al interaction, thin curve in Figure 6). On the other hand, in γ' containing Cr and Mn, x^B_{Al} continues to be very small (almost null) until the Al sublattice is filled up with Al atoms ($x_{Al} = 0.25$). The Ni-Cr interaction is less negative than the Ni-Al so that Cr or Mn atoms are squeezed out and, as a result, Al atoms stay in their own sublattice. The variation of x^B_{Al} with the composition in Cr or Mn added γ' is close to that in Cu added γ'.

It is noted that, in Figure 5, x^A_3 of Type III elements tends to decrease as x_{Ni} is increased from the stoichiometry. This is probably because the distinction of atom configurations in the two sublattices diminishes as more Ni atoms occupy the Al sublattice. As one goes farther in the Ni-rich side, the order-disorder transformation from metastable γ' to γ takes place.

In Figure 8 are shown the variations of x^A_3 with the bulk X concentration, X_3, in γ' which is at equilibrium with γ. x^A_3 is seen to increase almost linearly to x_3, which means that the X partitioning between the two sublattices is not much varied with the bulk X content.

B. γ'/γ *Phase Boundaries*

In Figures 9(a) through (d) are shown the calculated γ'/γ equilibrium phase boundaries in the isothermal section of the phase diagram of Ni-Al-Cr, Fe, Co, and Mo systems. Except for Co, experimentally determined phase boundaries are included.[34,35,36] In the calculation, the "BF" values in Table I(a) were used for the Ni-Al interaction parameters. As in the binary case, the Ni-X and Al-X interaction parameters obtained from the enthalpy and lattice parameter data usually did not reproduce the experimental phase boundaries in ternary systems. The best fit values of interaction parameters are determined by trial and error in some systems in the following manner: the change in e^0_{23} relative to e^0_{13} causing a small horizontal shift in the γ'/γ boundaries; also, the change in e^0_{33} alters the curvature of the boundaries as the X concentration is increased. The values thus determined (denoted "BF") are shown in the parentheses in Table I(b).

It is seen in these figures that for small concentrations of alloy elements the direction of γ'/γ phase boundaries correlates well with substitution behavior as originally pointed out by Guard and Westbrook.[12] Namely, in the Ni-Al-Co system the (γ' + γ) two phase field extends

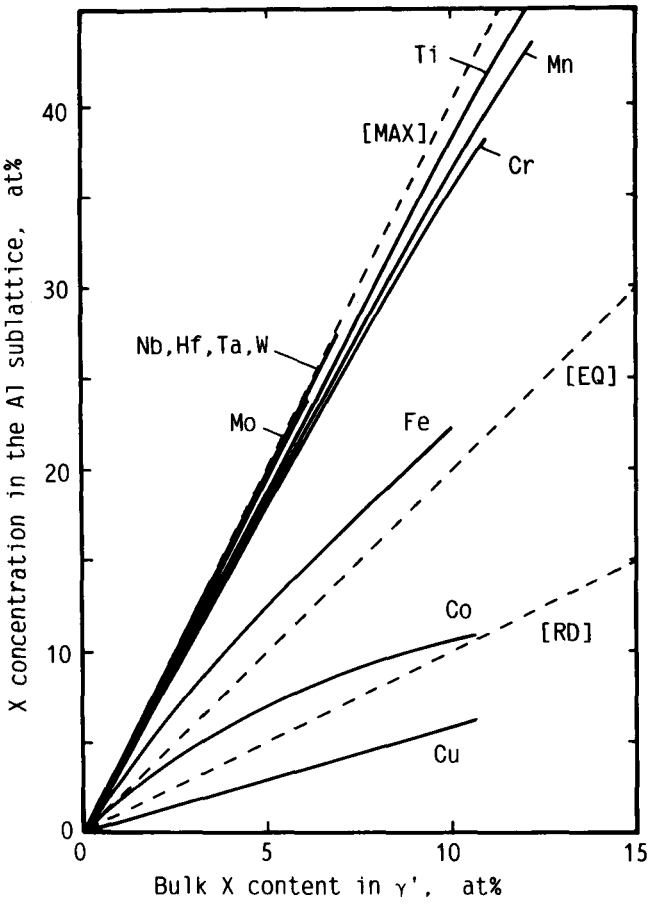

Fig. 8—Variation of alloy element concentration in the Al sublattice with the bulk concentration in γ' which is at equilibrium with γ.

nearly parallel to the Ni-Co side. As the fraction of substitution for Al sites is increased, the two phase field first tends to be upright (Cr and Fe) and leans toward the γ side (Mo) at relatively small concentrations.

It is noted that as the X concentration is increased, both the $\gamma'/(\gamma' + \gamma)$ and $\gamma/(\gamma' + \gamma)$ boundaries are often curved convex toward the γ side. Concomitantly, the slope of tie-lines appears to be increased. This seems to be consistent with the generally accepted rule that, at equilibrium, an alloy element tends to be enriched in the phase which is more stabilized than the other phase by the presence of it, and, thus, the phase field is widened relative to the other. However, this rule is unlikely to be obeyed strictly. As seen in Figures 9(b) and (c), both the experimental and calculated phase boundaries lean toward the γ side, rather than the γ' side, in spite of the fact that Cr (or Fe) is enriched in γ at equilibrium (see next section). Hence, in the case that one of the equilibrating phases is an ordered compound, the direction of phase boundaries appears to depend primarily upon substitution rather than partition (thus, stabilizing effect thereof) behavior of alloy elements.

C. *Partition Coefficient of Alloying Element between γ' and γ*

In Figures 10(a) through (g) are shown the variations of measured and calculated equilibrium partition coefficients of some alloy elements. The coefficient is defined as

$$k^{\gamma'/\gamma} = \frac{x_3^{\gamma'}}{x_3^{\gamma}} \qquad [12]$$

It is plotted against $x_3^{\gamma'}$ and x_3^{γ} for elements enriched in γ' and γ, respectively. The experimental data shown here were taken either from the diffusion couple measurement (white circles)[37] or by annealing in the two or three phase field (solid circles).[38] Dashed curves are calculated with the "BF" values.

The partition coefficient also appears to be affected by substitution behavior. Both experiment and calculation show that except Mo and W, Type II elements (here Ta, Figure 10(f)) are enriched in γ' ($k^{\gamma'/\gamma} > 1$), and the concentration dependence of $k^{\gamma'/\gamma}$ is rather small. In contrast, Types I and III elements are all enriched in γ ($k^{\gamma'/\gamma} < 1$), and the coefficients are usually dependent upon the concentration of alloy elements (Figures 10(a) through (d)).

These characteristics of partition behavior may be interpreted in terms of the atom configuration in the nearest neighbor shell. In Tables III(a) through (d) are shown the number of i-j pairs per lattice point, p_{ij}, the ratio of the number of i-j pairs to that of random distribution, σ_{ij}, and the number of j atoms in the first neighbor shell of an i atom, n_{ij}, in the binary and three ternary systems. These are written, respectively, as

$$p_{ii} = \frac{y_{ii}^{AB} + y_{ii}^{BB}}{2}, \quad p_{ij} = y_{ij}^{BB} + \frac{y_{ij}^{AB} + y_{ji}^{AB}}{2} \; (i \neq j) \qquad [13a]$$

$$n_{ij} = \frac{w_1}{2x_i}\left(y_{ij}^{BB} + \frac{y_{ij}^{AB} + y_{ji}^{AB}}{2}\right) \qquad [14a]$$

for γ' and

$$p_{ij} = y_{ij}, \quad p_{ij} = 2y_{ij} \; (i = j) \qquad [13b]$$

$$n_{ij} = w_1 \frac{y_{ij}}{x_i} \qquad [14b]$$

for γ. For both phases, σ_{ij} is written as,

$$\sigma_{ii} = \frac{p_{ii}}{x_i^2}, \quad \sigma_{ij} = \frac{p_{ij}}{2x_i x_j} \; (i \neq j) \qquad [15]$$

These quantities were calculated at equilibrium compositions of γ' and γ. However, for the sake of comparison, the alloy element concentrations were made equal in the two phases. Thus, these compositions are not the ones connected by a single tie-line. It is seen in Table III(a) that σ_{12} is increased upon ordering with concomitant decrease in σ_{11} and σ_{22} in the binary system. This indicates that, as usually expected, the probability of finding pairs of unlike atoms is increased upon $L1_2$ ordering. It is noted that n_{11} and n_{12} somewhat differ from the values of completely ordered γ' of stoichiometry composition (8 and 4, respectively) due to the larger Ni concentration in γ' at equilibrium with γ.

Of all the elements studied, Ta and Co exhibit the largest and the smallest $k^{\gamma'/\gamma}$, respectively. The first

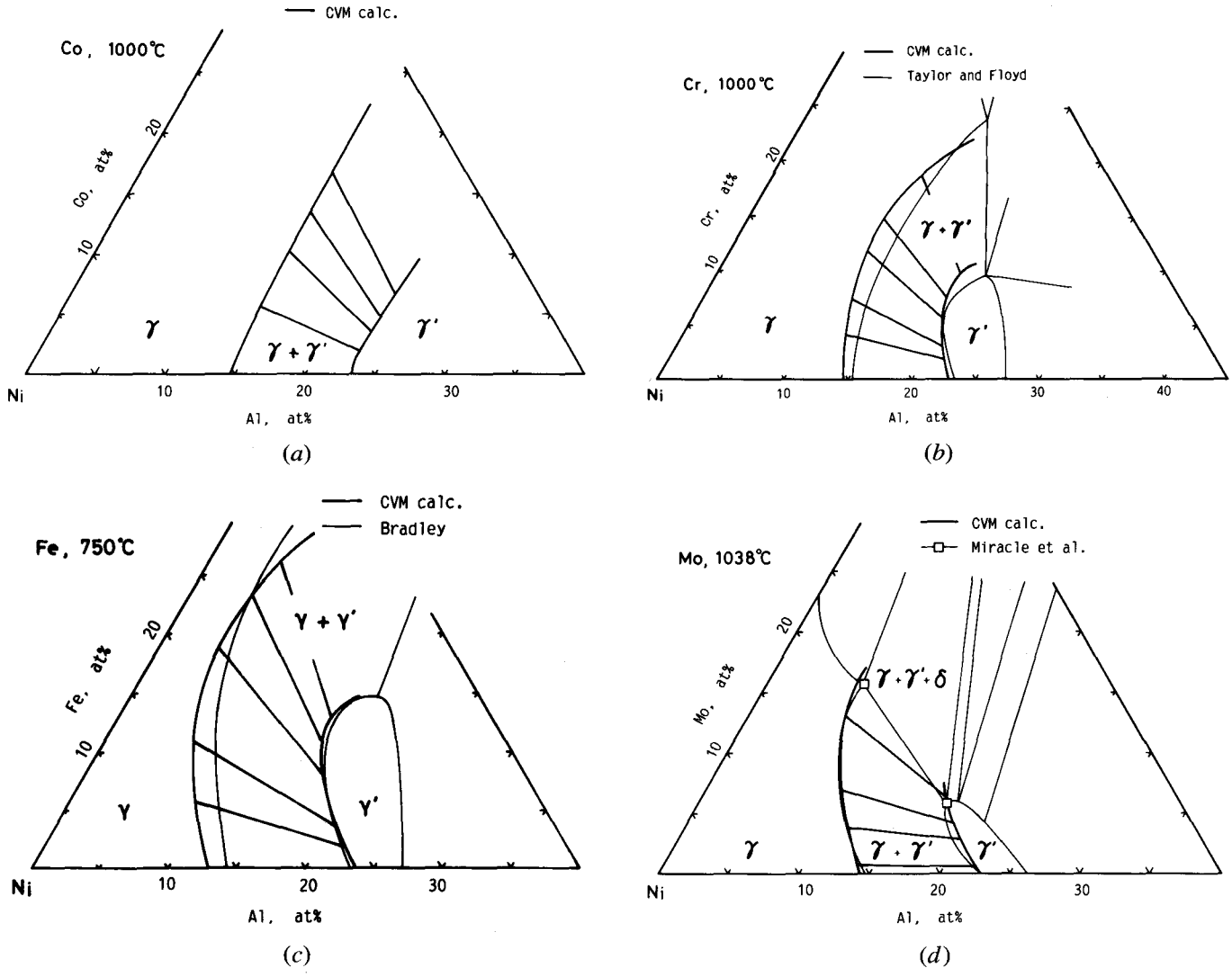

Fig. 9—γ'/γ phase boundaries in the isothermal section of the phase diagram of the (*a*) Ni-Al-Co; (*b*) Ni-Al-Cr; (*c*) Ni-Al-Fe; (*d*) Ni-Al-Mo systems. Experimental data were taken from Refs. 34 through 36.

neighbor atom configuration in these systems is shown in Tables III(b) and (c). The p_{ij} and so forth associated only with Ni and Al are not shown in these tables. They are not much different from the corresponding values in Table III(a). Because Ta is substituted for Al, the atom configuration in the first neighbor of Ta, n_{3j}, is almost the same as that of Al, n_{2j}, in γ'. These are even similar in the two phases. The enrichment of Ta in γ' may be attributed to the larger σ_{13} value (1.29) in γ' compared to that in γ (1.16), just like σ_{12} in the binary systems. As a result, the substitution for Al sites necessitates the enrichment in γ' because strongly attractive Ni-X pairs are formed more readily in γ' than in the other phase.

Because Co atoms enter in both sublattices of γ', the situation is more complex. However, there is a remarkable difference in the nearest neighbor atom configuration. Namely, whereas two Al atoms are present in the first neighbor shell of Co in γ' ($n_{32} = 2.0$), approximately only one Al atom can enter the first neighbor in γ ($n_{32} = 1.2$). Hence, the enrichment of Co in γ' is unfavored because more Co-Al pairs, whose interaction is less negative than the others (Table III(c)) and thus is relatively unstable, are formed than in γ. Similar atom configurations are obtained in other systems of Types I and III elements.

The measured $k^{\gamma'/\gamma}$ of Mo is seen to depend remarkably upon the Mo concentration; whereas Mo is enriched in γ' at small concentrations, the reverse is true at larger concentrations (Figure 10(e)). The dashed curve is seen to reproduce fairly well the concentration dependence of $k^{\gamma'/\gamma}$ of Mo. Whether W is enriched in γ' or γ is not well established. The solid circles in Figure 10(g) indicate the same concentration dependence of $k^{\gamma'/\gamma}$ of W as that of Mo. The Type II elements, such as Ta, are usually characterized by a combination of large e^0_{33} and r_{33} values. They may be weakly attractive, or even repel each other in the γ' and γ lattices because of the rapidly rising first term in the L-J potential. In contrast, Mo and W can have very strong attractive self interactions in γ. As shown in Table III(d), a significant amount of Mo-Mo pairs are already present in γ at 5 at. pct Mo level ($n_{33} = 0.6$) and its proportion may increase as the bulk content of

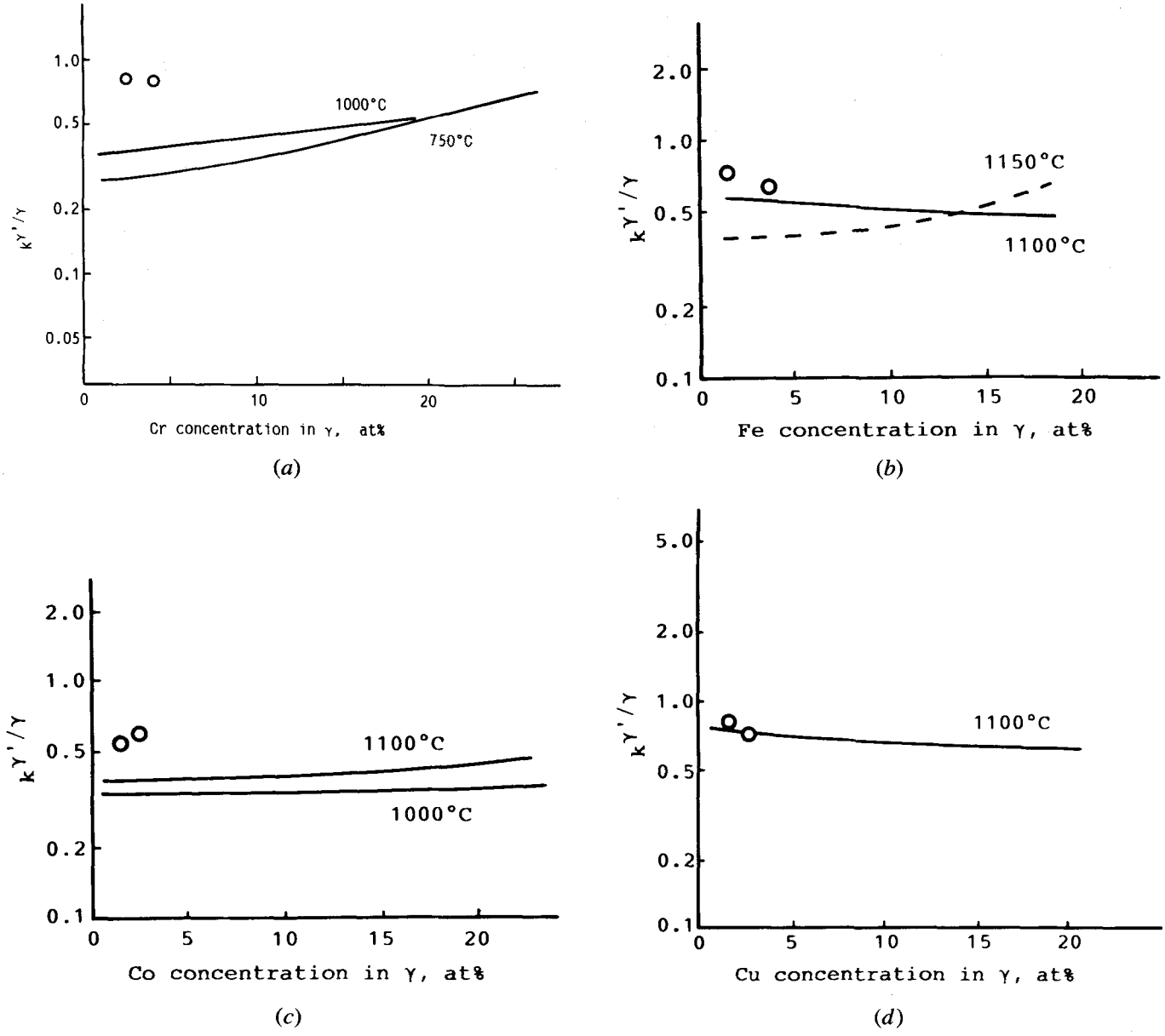

Fig. 10—Variation of equilibrium partition coefficient, $k^{\gamma'/\gamma}$, with the alloy element concentration for (*a*) Cr; (*b*) Fe; (*c*) Co; (*d*) Cu; (*e*) Mo; (*f*) Ta; (*g*) W. White circles are the data by diffusion couple measurements at 1100 °C.[36] Black circles are the data taken by two-phase annealing at 1000 °C or by three-phase annealing at 900 °C.[37]

Mo is increased. On the other hand, since Mo (and presumably W) is substituted for Al, very few Mo-Mo pairs can exist in γ' ($n_{33} = 0.1$). This may result in progressively larger Mo enrichment in γ, exactly the tendency observed in the dashed curve of Figure 10(e).

D. *Order-Disorder Transformation Temperature of γ'*

It has long been questioned whether γ' is completely ordered up to its melting temperature. The order parameter of Ni_3Al was measured by high temperature X-ray diffractometry.[39] Recently, Cahn *et al.*[40,41] succeeded in determining the temperature of the order-disorder transformation from metastable γ' to γ (it is denoted as T_{OD}, hereafter) in Ni-Al-Fe alloys by a combination of thermal dilatometry and X-ray diffractometry. It was then suggested that the relative position of the transformation temperature and the liquidus of metastable γ' controls the formation of fine antiphase domain structure upon solidification and profoundly affects the ductility of γ'. The locus of this transformation temperature in the binary system, which appears to fall in the ($\gamma' + \gamma$) two phase field, represents an upper limit of γ' existence if nucleation of γ is suppressed for some reason. Thus, the evaluation of T_{OD} may have an important practical significance.

In Figure 11 are compared calculated and measured[40] T_{OD} of γ' which contain 12.5 at. pct Fe. The "BF" values in Table I(a) yielded the transformation temperature of 1685 °C for binary γ' of stoichiometry composition,

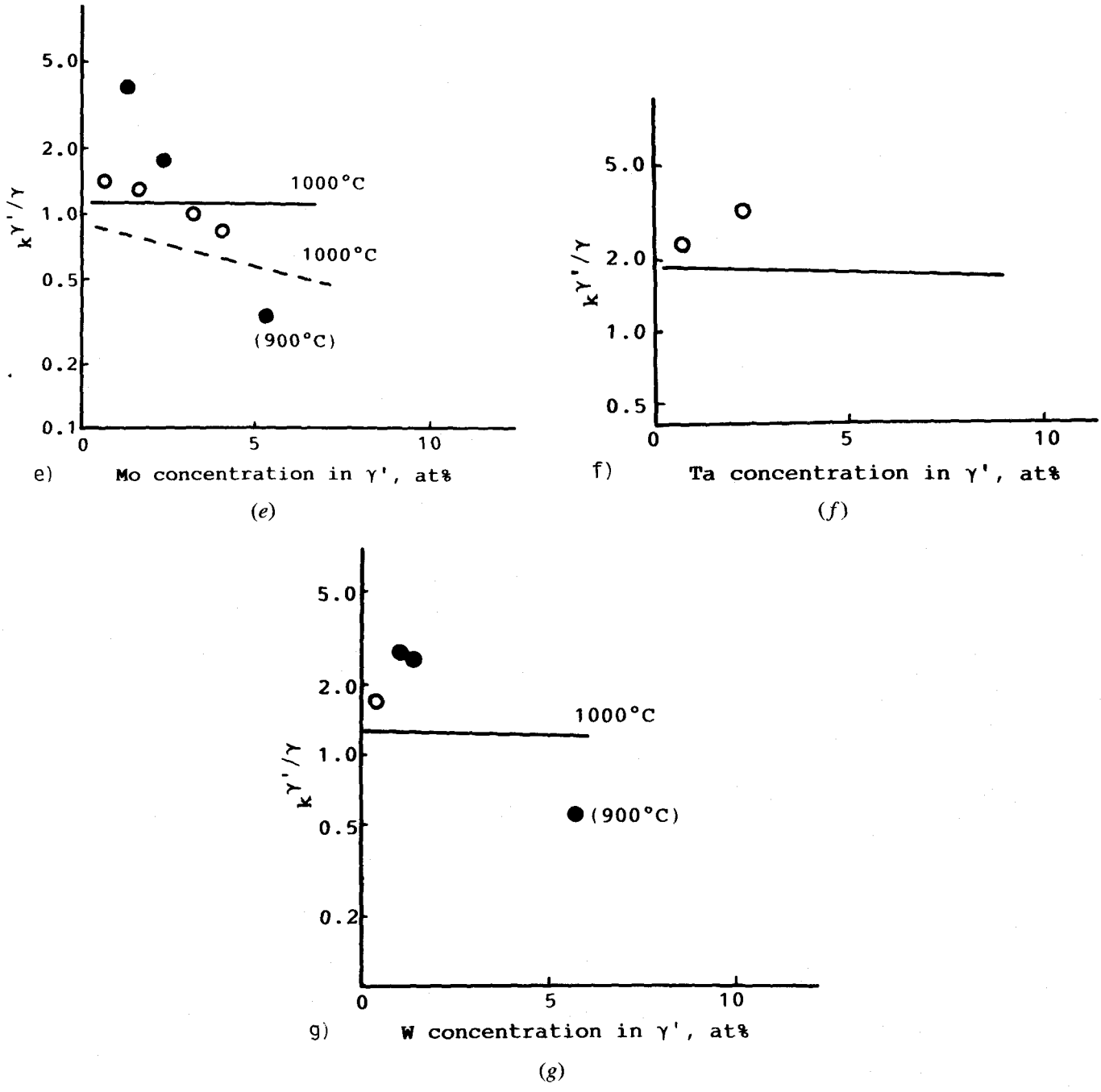

Fig. 10 Cont.—Variation of equilibrium partition coefficient, $k^{\gamma'/\gamma}$, with the alloy element concentration for (*a*) Cr; (*b*) Fe; (*c*) Co; (*d*) Cu; (*e*) Mo; (*f*) Ta; (*g*) W. White circles are the data by diffusion couple measurements at 1100 °C.[36] Black circles are the data taken by two-phase annealing at 1000 °C or by three-phase annealing at 900 °C.[37]

which is about 200 °C higher than that reported by Cahn *et al.*[40] Though this trend is inherent in the figure, the qualitative features of the calculated variation of T_{OD} with the Ni/Al ratio agree well with measurements.

Figure 12 shows the calculated variation of T_{OD} with the bulk concentration of various alloy elements. The curves are drawn for constant Ni-Al ratio (=75/25) for Fe and Cu and for constant Ni concentration for Nb and Mo. It is apparent that, whereas Nb raises T_{OD}, Cu and Fe lower it. The addition of Mo raises T_{OD} initially, but lowers it at larger concentrations. These variations appear to be related closely to partition behavior of each element. Hence, the influence of alloy element addition upon T_{OD} may be attributed primarily to its influence upon the thermodynamic stability of γ' relative to that of γ.

E. *Effects of Alloy Element Addition upon Lattice Constants*

The mismatch in lattice parameter between γ' and γ is one of the most important parameters for the design of creep and heat resistant Ni-base superalloys. In

Table III. Calculated Numbers of *i-j* Pairs Per Lattice Point, p_{ij}, Ratios of the Numbers of *i-j* Pairs to Those of Random Distribution, σ_{ij}, and Numbers of *j* Atoms in the First Neighbor Shell of an *i* Atom, n_{ij}, in Binary and Three Ternary γ' and γ, in (a) Ni-Al, (b) Ni-Al-Ta, (c) Ni-Al-Co, and (d) Ni-Al-Mo Systems. The Atom Fraction of X in Each Phase Is the Same.

(a)

	Ne_{ij}, kcal/mol		γ':$Ni_{77}Al_{23}$		γ:Ni-14Al	
			p_{ij}	σ_{ij}	p_{ij}	σ_{ij}
Ni-Ni	−17.1		0.56	0.92	0.70	0.97
Ni-Al	−17.8		0.44	1.28	0.29	1.15
Al-Al	− 7.2		0.00	0.00	0.00	0.07
	n_{ij}	i	j: Ni	Al	Ni	Al
		Ni	8.6	3.4	9.9	2.1
		Al	12.0	0.0	11.8	0.2

(b)*

	Ne_{ij}, kcal/mol		γ':$Ni_{78}Al_{17}Ta_5$			γ:Ni-9Al-5Ta		
			p_{ij}	σ_{ij}		p_{ij}	σ_{ij}	
Ni-Ta	−29.1		0.10	1.29		0.10	1.16	
Al-Ta	−10.3		0.00	0.00		0.00	0.00	
Ta-Ta	− 6.8		0.00	0.00		0.00	0.00	
	n_{ij}	i	j: Ni	Al	Ta	Ni	Al	Ta
		Ni	8.5	2.7	0.8	10.1	1.2	0.7
		Al	12.0	0.0	0.0	11.9	0.1	0.0
		Ta	12.0	0.0	0.0	12.0	0.0	0.0

(c)

	Ne_{ij}, kcal/mol		γ': $Ni_{69}Al_{21}Co_{10}$			γ: Ni-13Al-10Co		
			p_{ij}	σ_{ij}		p_{ij}	σ_{ij}	
Ni-Co	−17.1		0.13	0.98		0.16	1.02	
Al-Co	−15.6		0.04	0.83		0.02	0.77	
Co-Co	−17.1		0.01	1.56		0.01	1.21	
	n_{ij}	i	j: Ni	Al	Co	Ni	Al	Co
		Ni	7.5	3.3	1.2	9.0	2.0	1.0
		Al	11.0	0.0	1.0	11.0	0.1	0.9
		Co	8.0	2.0	2.0	9.4	1.2	1.4

(d)

	Ne_{ij}, kcal/mol		γ': $Ni_{77}Al_{18}Mo_5$			γ: Ni-10Al-5Mo		
			p_{ij}	σ_{ij}		p_{ij}	σ_{ij}	
Ni-Mo	−21.8		0.10	1.28		0.09	1.12	
Al-Mo	− 9.9		0.00	0.00		0.00	0.04	
Mo-Mo	−22.6		0.00	0.29		0.00	0.98	
	n_{ij}	i	j: Ni	Al	Mo	Ni	Al	Mo
		Ni	8.4	2.9	0.7	9.9	1.5	0.6
		Al	12.0	0.0	0.0	11.8	0.2	0.0
		Mo	11.7	0.0	0.1	11.3	0.1	0.6

*The p_{ij} and σ_{ij} values for Ni and Al pairs are not included in (b) through (d). They are not much different from the values in (a).

Figure 13 is shown the variation of lattice constant of the two phases (denoted as $a_{\gamma'}$ and a_{γ}) with the composition of the binary phases calculated with the use of three sets of parameter values shown in Table I(a). As expected, the "BF" values yield remarkably larger $a_{\gamma'}$ and a_{γ} than the measured ones.[22] The $a_{\gamma'}$ curve was calculated under the same assumption as before, *i.e.*, absence of structural vacancies. The curve is seen to have an inflection at the stoichiometry, because the excess Al atoms which enter the Ni sublattice form Al-Al pairs and tend to expand the lattice (because of a large r_{22} value). The same is true with a_{γ}, probably because of the similarities of the first neighbor atom configuration (or the short range order) between the two phases (n_{21} = 12.0 and 11.8 in γ' and γ, respectively, Table II(a)). It is noted that a_{γ} is slightly larger than $a_{\gamma'}$ at the same

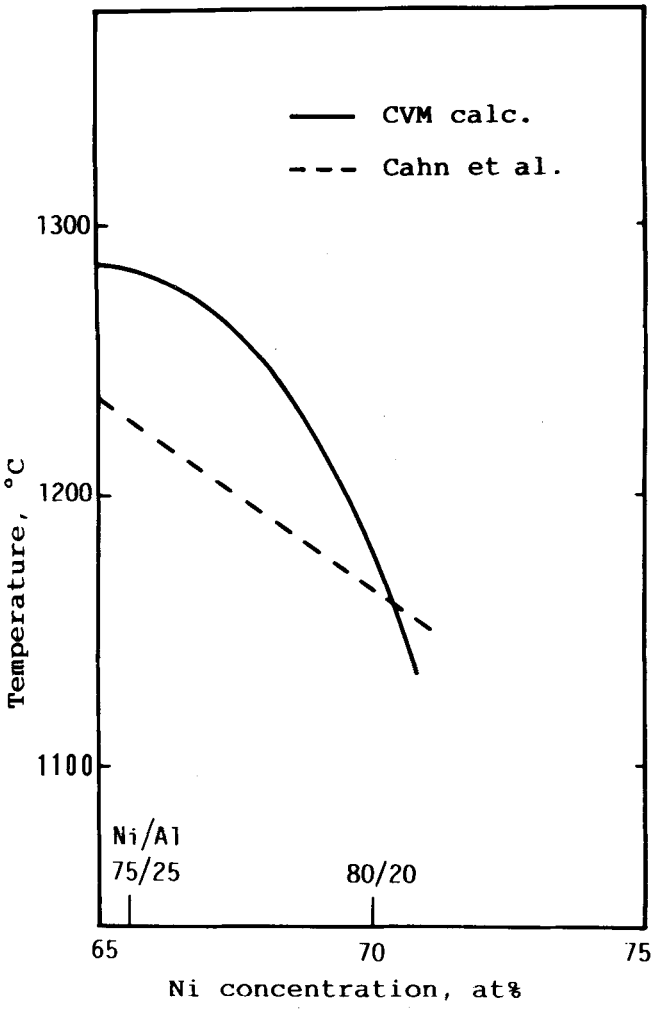

Fig. 11—Comparison of calculated and measured[40] order-disorder transformation temperature, T_{OD}, from metastable γ' to γ, which contains 12.5 at. pct Fe.

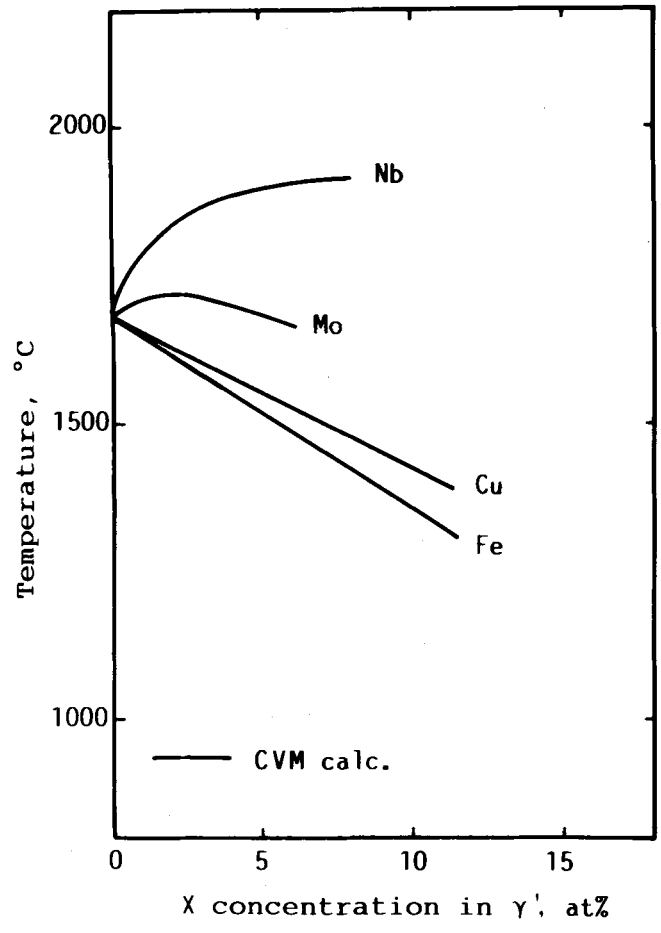

Fig. 12—Variation of calculated order-disorder transformation temperature with the alloy element concentration.

composition. This can be ascribed to the larger number of Al-Al pairs in γ than in γ' (σ_{22} = 0.07 and 0.00 in γ and γ', respectively).

In comparing lattice constants with experiment in ternary systems, it is necessary to check whether the data were taken from a single phase alloy or from a γ'/γ mixture. The latter data must be compared with those at the proper phase boundary compositions. Accordingly, the analysis was made with the use of the "BF" values and the results were corrected for the ratio (0.983) which compensates for the difference between the curves [γ'] and [BF].

Figure 14(a) shows the variation of calculated and measured[42] $a_{\gamma'}$ and a_{γ} with the Hf content. The initial compositions (x_{Hf} = 0) are the ones at binary equilibrium. Solid curves are the variations along the ternary equilibrium boundaries and dashed curves for constant Al concentration. Both a_{γ} and $a_{\gamma'}$ are increased at a larger rate in the dashed curves than in the solid curves. This is because the addition of Hf removes almost an equal number of Al atoms along the equilibrium boundary. The inflection of the $a_{\gamma'}$ curve at $x_{Hf} \sim 0.02$ may occur for the same reason as that in the binary case, but the slope is larger because of the formation of Hf-Al pairs (and Al-Al pairs as well) between the two sublattices.

It can be shown that the $a_{\gamma'}$ curve for Type III elements, such as Cr, exhibits the same inflection at the stoichiometry composition. However, the degree of inflection for these elements is smaller than for Type II elements, due to relatively small differences in the atomic radii from that of Ni. No inflection appears for Type I elements.

The variations of $a_{\gamma'}$ and a_{γ} with the Mo concentration are shown in Figure 14(b). The experimental data shown here were taken from the two phases which were supposed to be at equilibrium.[43] Although for most other elements the lattice constant of γ is smaller than that of γ', the reverse is true with Mo. The calculated variations are seen to be in fair agreement with this observation. The fact that a_{γ} increases at an increasing rate with the Mo concentration may be ascribed to the combination of large enrichment and tendency to form Mo-Mo pairs in γ, as mentioned in Section III–C.

Figures 15(a) and (b) show the variations of calculated $a_{\gamma'}$ and a_{γ} with the concentration for all alloy elements studied. The calculation was performed at 1000 °C. Type II elements are usually large in the atomic radius, and thereby the rate of increasing the lattice constants tends to be large. The appearance of the variation of lattice constants with the alloy element concentration does not differ much in these two phases.

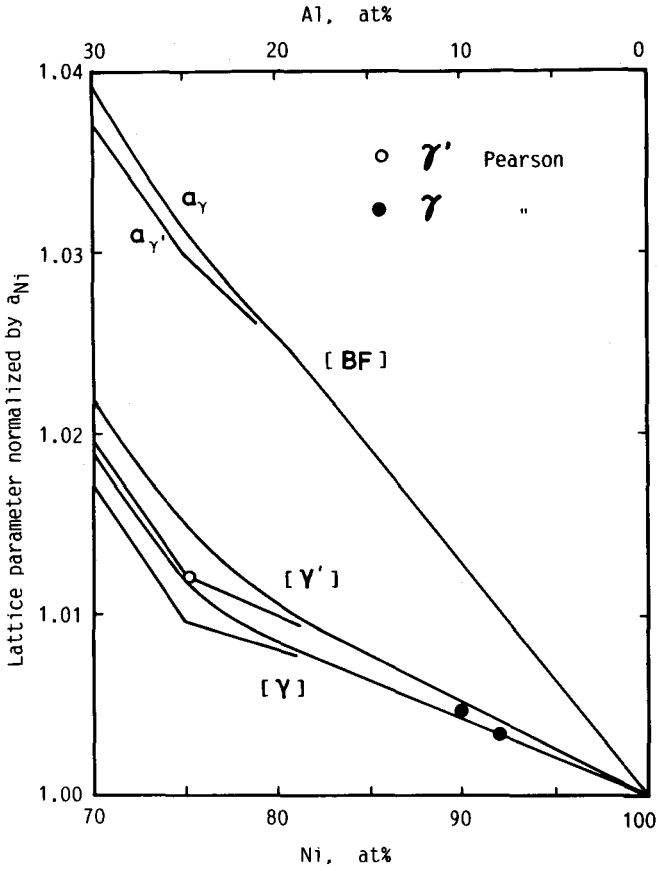

Fig. 13—Lattice constant of binary γ' and γ calculated with the use of the three sets of Ni-Al potential parameters in Table I(a).

IV. SUMMARY

The cluster variation method (CVM) with the Lennard-Jones pair potential was used to analyze substitution behavior of alloy elements in γ', γ'/γ equilibrium phase boundaries, equilibrium partition coefficient, order-disorder transformation temperature from metastable γ' to γ and lattice constants in eleven ternary Ni-Al-X (X = Ti, Cr, Mn, Fe, Co, Cu, Nb, Mo, Hf, Ta, and W) systems. The values of the potential parameters were determined primarily from the thermochemical data on enthalpy and the data on lattice constants of metals, binary alloys, and compounds. For systems in which no appreciable data appear to be available, empirical laws were utilized.

The following conclusions may be drawn:

1. Substitution behavior of alloy elements in γ' is classified into three types. The elements whose interactions with Ni and Al are similar in magnitude are substituted preferentially for Ni sites (Type I, Co, and Cu). The elements whose interaction with Ni is much stronger than with Al are almost entirely substituted for Al sites (Type II, Ti, Nb, Mo, Hf, Ta, and W). The substitution site of the other elements, of which the differences in the magnitude of interactions are intermediate, is highly dependent upon the bulk composition of γ' (Type III, Cr, Mn, and Fe); whereas they are substituted for Al when the sum of the Al

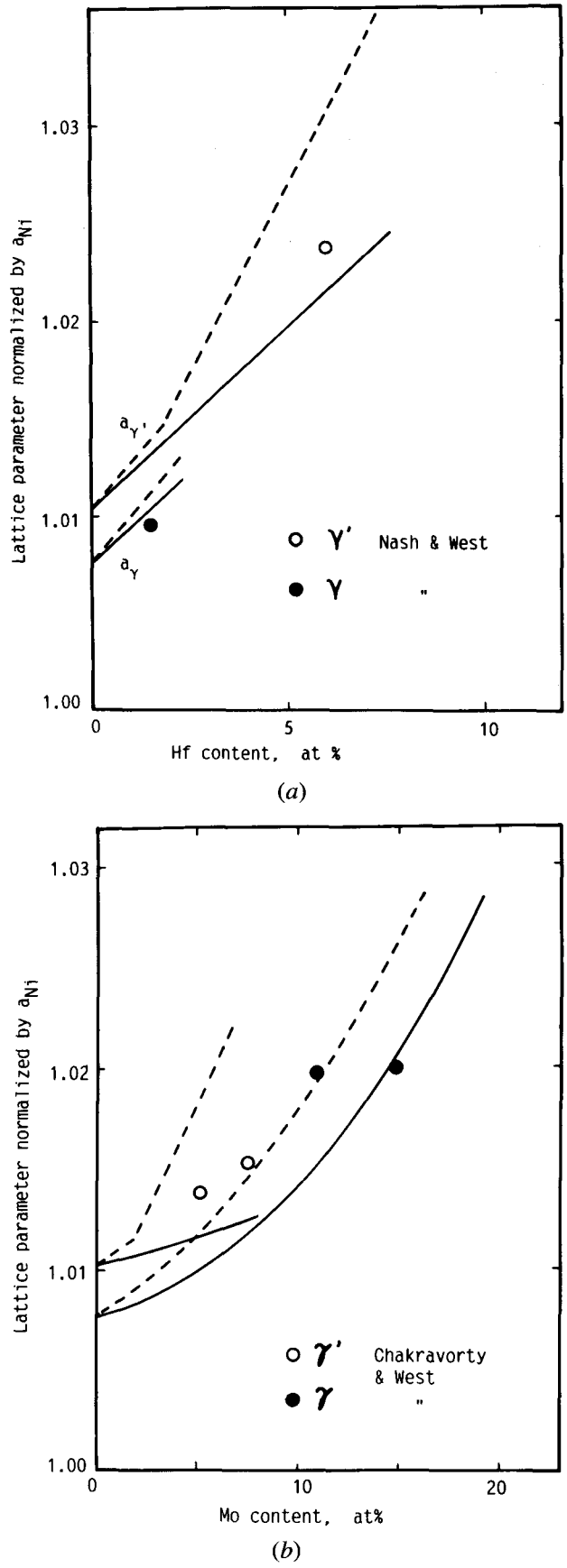

Fig. 14—Variation of lattice constant of γ' and γ with the (*a*) Hf and (*b*) Mo concentrations. Solid and dashed curves are, respectively, the variations along the phase equilibrium compositions and for constant Al concentration. Data were taken from Refs. 42 and 43.

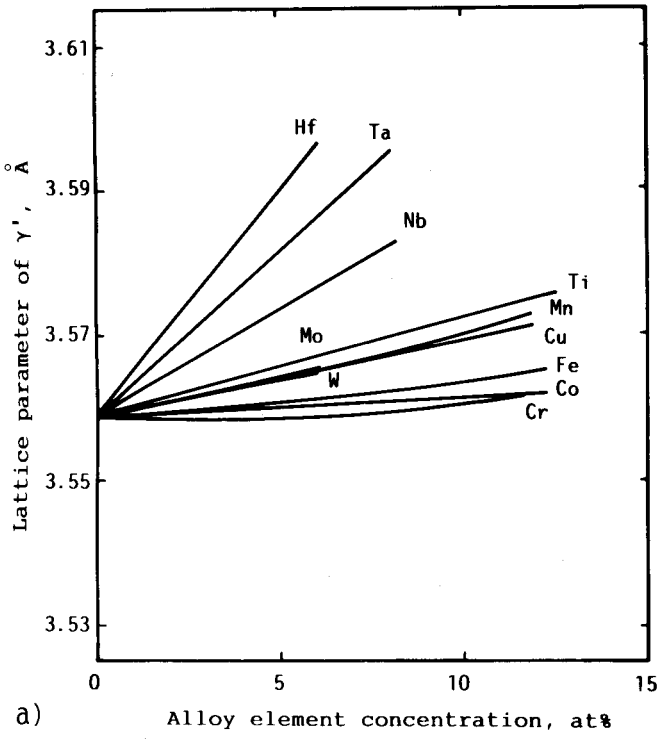

(*a*)

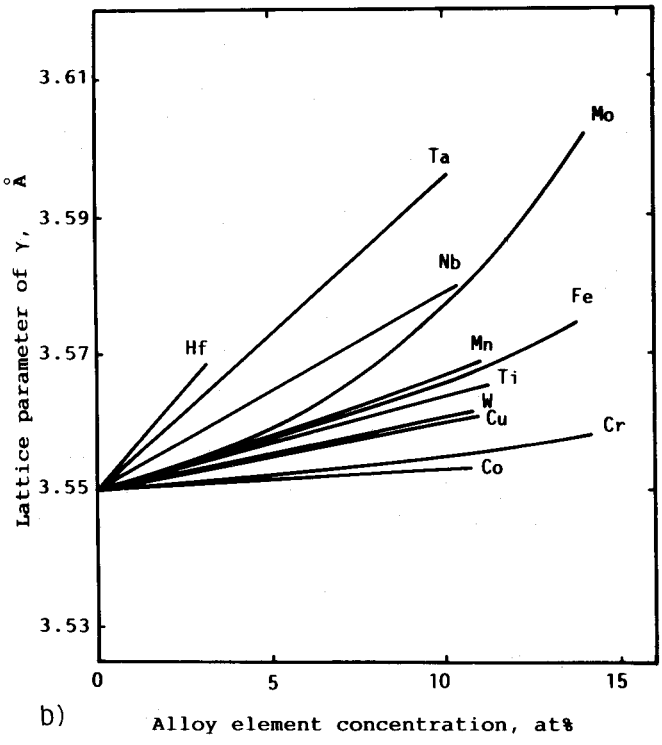

(*b*)

Fig. 15—Effects of alloy element addition upon lattice constant of (*a*) γ'; (*b*) γ.

and X concentrations are less than the stoichiometry composition, they begin to enter the Ni lattice as soon as the sum of the two concentration exceeds it. For some elements such as Fe and Cr, the calculated occupancy fractions in the sublattices are in good agreement with those measured by ALCHEMI and Mössbauer spectroscopy.

2. The direction of extention of the ($\gamma' + \gamma$) two phase field appears to be related to substitution behavior. The Type I elements have the two phase field parallel to the Ni-X side in the isothermal section of the ternary phase diagram and the Type II elements, parallel to the Al-X side. The direction of the two phase field of the Type III elements is intermediate between the above two types. However, the two phase field of these elements is usually curved convex toward the γ' side as the X concentration is increased. Some Type II elements, *e.g.*, Mo, exhibit a two phase field similar to that of Type III elements.
3. Most Type II elements are enriched in γ' at two phase equilibrium. This is probably because the probability of forming Ni-X pairs of strong attractive interaction is increased in the $L1_2$ ordered lattice than in the solid solution of γ. The Type I and Type III elements are enriched in γ, which may also be explained from the atom configuration in the nearest neighbor shell. The partition coefficient of Mo and presumably W is highly concentration dependent.
4. The effects of alloying elements upon the order-disorder transformation temperature from metastable γ' to γ appear to be related to their partition behavior. The temperature is raised by the addition of Type II elements (except for large concentrations of Mo) and decreased by the addition of Types I and III elements.
5. The Type II elements, whose atomic radius is relatively large, increase the lattice constants of both γ' and γ at a larger rate than the other elements. Though the lattice constant of γ' is usually larger than that of γ, the reverse situation can occur in some systems such as Mo, characterized by a large enrichment in γ and a relatively large atomic radius.

ACKNOWLEDGMENT

The authors are grateful to Dr. M. Yamazaki, Director of Materials Design Division, National Research Institute for Metals, for valuable discussions.

REFERENCES

1. L. Kaufman and H. Nesor: *CALPHAD*, 1978, vol. 2, pp. 325-48.
2. L. Kaufman and H. Bernstein: *Computer Calculation of Phase Diagrams*, Academic Press, New York, NY, 1970.
3. L. Kaufman and H. Nesor: *Metall. Trans.*, 1974, vol. 5, pp. 1617-21, pp. 1623-29; 1975, vol. 6A, pp. 2115-22, pp. 2123-31.
4. L. Kaufman and H. Nesor: *Can. Metall. Q.*, 1975, vol. 14, pp. 221-32.
5. J.M. Sanchez, J.R. Barefoot, R.N. Jarrett, and J.K. Tien: *Acta Metall.*, 1984, vol. 32, pp. 1519-25.
6. T. Mohri and K. Watanabe: *Transactions of the Iron and Steel Institute of Japan*, 1988, vol. 28, pp. 783-94.
7. C. Sigli and J.M. Sanchez: *Acta Metall.*, 1985, vol. 33, pp. 1097-104.
8. C. Sigli and J.M. Sanchez: *Acta Metall.*, 1986, vol. 34, pp. 1021-28.
9. H. Harada, M. Yamazaki, Y. Koizumi, N. Sakuma, and N. Furuya: *High Temperature Alloys for Gas Turbines*, Conf. Proc., D. Reidel Publishing Company, Boston, MA, 1982, pp. 721-35.
10. H. Harada, K. Ohno, T. Yamagata, T. Yokokawa, and M.

Yamazaki: *6th Int. Symp. Superalloys*, 18 through 22 Sept., Seven Springs, PA, 1988.
11. J.K. Tien: *Proc. Japan-US Seminar on Superalloys*, Japan Institute for Metals, Fuji Susono, Japan, 1984, pp. 333-51.
12. R.W. Guard and J.H. Westbrook: *Trans. TMS-AIME*, 1959, vol. 215, pp. 807-14.
13. J.W. Drijver and F. Van der Woude: *J. Phys. (F)*, Metal Phys., 1973, vol. 3, pp. L206-L211.
14. J.R. Nichols and R.D. Rawlings: *Acta Metall.*, 1977, vol. 25, pp. 187-94.
15. D. Shindo, M. Hirabayashi, S. Hanada, and O. Izumi: *Preprints 100th Spring Meeting of Japan Institute for Metals*, 1987, p. 292.
16. S. Ochiai, Y. Oya, and T. Suzuki: *Bulletin of Precision Machinery*, Tokyo Institute of Technology, 1983, no. 52, pp. 1-17.
17. C. Sigli and J.M. Sanchez: *CALPHAD*, 1984, vol. 8, pp. 220-31.
18. R. Furth: *Proc. Roy. Soc.*, 1944, vol. 183A, pp. 87-110.
19. R. Kikuchi and D. de Fontaine: *NBS special publications, SP-496*, Gaitherburg, MD, 1977, pp. 967-1026.
20. R. Hultgren, P.D. Desai, D.T. Hawkins, M. Gleiser, K.K. Kelley, and D.D. Wagman: *Selected Values of the Thermodynamic Properties of the Elements*, ASM, Metals Park, OH, 1973.
21. R. Hultgren, P.D. Desai, D.T. Hawkins, M. Gleiser, K.K. Kelley, and D.D. Wagman: *Selected Values of the Thermodynamic Properties of the Alloys*, ASM, Metals Park, OH, 1973.
22. W.B. Pearson: *A Handbook of Lattice Spacing and Structure of Metals and Alloys*, Pergamon Press, London, 1967, vol. 2.
23. P. Villars and L.D. Calvert: *Pearson's Handbook of Crystallographic Data for Intermetallic Phases*, ASM, Metals Park, OH, 1985, vols. 2 and 3.
24. L. Kaufman: *CALPHAD*, 1978, vol. 2, pp. 117-46; 1979, vol. 3, p. 45-76.
25. L. Kaufman and H. Nesor: *CALPHAD*, 1978, vol. 2, pp. 55-80, pp. 81-108, pp. 295-318.
26. H.W. King: *J. Mater. Sci.*, 1966, vol. 1, pp. 79-90.
27. A.R. Miedema, F.R. de Boer, and R. Room: *CALPHAD*, 1977, vol. 1, pp. 341-59.
28. A.R. Miedema and P.F. de Chatel: *Theory of Alloy Phase Formation*, L.H. Bennett, ed., TMS-AIME, 1979, pp. 344-89.
29. R.D. Rawlings and A.E. Staton-Bevan: *J. Mat. Sci.*, 1975, vol. 10, pp. 505-14.
30. M.P. Arbuzov, E.T. Kachkovskaya, and B.V. Khayenko: *Fiz. Met. Metallv.*, 1966, pp. 854-57.
31. A.V. Karg, D.E. Fornwalt, and O.H. Kriege: *J. Inst. Metals*, 1971, vol. 99, pp. 301-05.
32. O.H. Kriege and J.M. Baris: *Trans. ASM*, 1969, vol. 62, pp. 195-200.
33. N. Brown: in *Intermetallic Compounds*, J.H. Westbrook, ed., John Wiley & Sons Inc., New York, NY, 1979, p. 269.
34. A. Taylor and R.W. Floyd: *J. Inst. Metals*, 1952–1953, vol. 81, pp. 451-64.
35. A.J. Bradley: *J. Iron Steel Inst.*, 1949, vol. 163, p. 1930; 1951, vol. 168, pp. 233-44.
36. D.B. Miracle, K.A. Lack, V. Srinivasan, and H.A. Lipsitt: *Metall. Trans. A*, 1984, vol. 15A, pp. 481-86.
37. C.-C. Jia, K. Ishida, and T. Nishizawa: *Preprints 98th Spring Meeting of Japan Inst. Metals*, Tokyo, 1986, p. 328.
38. M. Enomoto, H. Harada, and Y. Hakamazuka: National Research Institute for Metals, Tsukuba, Japan, 1987, unpublished research.
39. R.W. Guard and J.H. Westbrook: *Trans. TMS-AIME*, 1959, vol. 215, pp. 871-72.
40. R.W. Cahn, P.A. Siemers, J.E. Geiger, and P. Bardhan; *Acta Metall.*, 1987, vol. 35, pp. 2737-51.
41. R.W. Cahn, P.A. Siemers, and E.L. Hall: *Acta Metall.*, 1987, vol. 35, pp. 2753-64.
42. P. Nash and D.R.F. West: *Met. Sci.*, 1981, vol. 15, pp. 347-52.
43. S. Chakravorty and D.R.F. West: *Met. Sci.*, 1984, vol. 18, pp. 207-15.